Geophysical Research Letters

RESEARCH LETTER
10.1029/2024GL109466

Separate the Role of Southern and Northern Extra-Tropical Pacific in Tropical Pacific Climate Variability

Yingying Zhao[1], Daoxun Sun[1], Emanuele Di Lorenzo[2], Guangpeng Liu[3], and Sheng Wu[4]

[1]Laoshan Laboratory, Qingdao, China, [2]Department of Earth, Environmental, and Planetary Sciences, Brown University, Providence, RI, USA, [3]The State Key Laboratory of Estuarine and Coastal Research, East China Normal University, Shanghai, China, [4]Laboratory for Climate and Ocean-Atmosphere Studies & Department of Atmospheric and Oceanic Sciences, School of Physics, Peking University, Beijing, China

Key Points:

- The SEP dynamics contribute ~40% of the tropical interannual variance and ~70% of the southeastern tropical low-frequency variance
- The NEP dynamics do not impact the tropical interannual variance but lead to ~70% of the central tropical low-frequency variability
- CMIP6 models show stronger NEP (SEP) dynamics tend to manifest ENSO with more (less) low-frequency (>6 years) power

Supporting Information:

Supporting Information may be found in the online version of this article.

Correspondence to:

D. Sun,
dxsun@qnlm.ac

Citation:

Zhao, Y., Sun, D., Di Lorenzo, E., Liu, G., & Wu, S. (2024). Separate the role of southern and northern extra-tropical Pacific in tropical Pacific climate variability. *Geophysical Research Letters*, *51*, e2024GL109466. https://doi.org/10.1029/2024GL109466

Received 25 MAR 2024
Accepted 3 AUG 2024

Abstract Observational and modeling studies have elucidated the influential role played by the southern and northern extratropical Pacific (SEP and NEP) forcing in shaping dynamics of tropical Pacific climate variability. However, the relative importance of the NEP and SEP and the timescale on which they impact the tropics remain unclear. Using a linear inverse model (LIM) that selectively incorporates or excludes tropical-extratropical coupling, we find a reduction in tropical interannual variability (~40%) and low-frequency (sub-decadal to decadal) variability in the southeastern tropical Pacific region (~70%) in the absence of SEP. Conversely, the absence of NEP yields no significant impact on tropical interannual variability but markedly diminishes low-frequency variability in the central tropical Pacific region (~70%). LIM and statistic diagnostics on CMIP6 models show the low-frequency to total variability ratio in the tropical Pacific depending on their NEP and SEP representation. Models with more (less) low-frequency power tend to show stronger NEP (SEP) dynamics.

Plain Language Summary The tropical Pacific climate variability exerts a strong impact on global climate, regional weather, and marine ecosystems. The tropical and extratropical Pacific are closely coupled with each other through oceanic and atmospheric processes. Previous studies have shown that the southern and northern extratropical Pacific (SEP and NEP) forcing greatly impact the tropical Pacific climate variability. To understand and predict tropical Pacific variability, it is necessary to study the relative importance and the timescale on which the SEP and NEP exert their influence. In this study, we use an empirical dynamical model to exclude the impacts of SEP or NEP on the tropical Pacific based on the observational data. We find that the absence of SEP leads to a significant reduction of interannual variance (~40%) and the low-frequency (sub-decadal to decadal) variance in the southeastern tropical Pacific region (~70%), while the absence of the NEP does not change the interannual variance but significantly reduces the low-frequency variance in the central tropical Pacific region (~70%). In observations, the ratio of low-frequency to total tropical variability is 0.36, while CMIP6 models exhibit a wider range, with enhanced low (high) frequency power associated with stronger NEP (SEP) dynamics.

1. Introduction

The tropical Pacific climate variability, including the El Niño-Southern Oscillation (ENSO) and the tropical Pacific decadal variability (TPDV), exerts an important impact on global climate, regional weather, and marine ecosystems, particularly over North America and Asia with important societal impacts (Alexander et al., 2002; Capotondi et al., 2020; Di Lorenzo et al., 2013; Fisman et al., 2016; Z. Liu & Di Lorenzo, 2018). The tropical Pacific and extra-tropical Pacific are strongly coupled with each other. Notably, the extratropical ENSO precursors, such as the seasonal footprinting mechanism (SFM) (Vimont et al., 2001, 2003a, 2003b), the trade wind charging (TWC) mechanism (Anderson, 2003; Anderson et al., 2013), the North and South Pacific Meridional Modes (NPMM, Chiang & Vimont, 2004, and SPMM, Zhang et al., 2014), have proven highly effective in influencing both ENSO (e.g., Alexander et al., 2010; Chang et al., 2007; Larson & Kirtman, 2013, 2014; T. Liu et al., 2024; Thomas & Vimont, 2016; You & Furtado, 2017; Zhang, Chang, & Ji, 2009; Zhang, Chang, & Tippett, 2009) and tropical Pacific decadal variability (e.g., Chung et al., 2019; Di Lorenzo et al., 2015; Liguori & Di Lorenzo, 2018; Liguori & Di Lorenzo, 2019; Sun & Okumura, 2019; Zhang et al., 2014; Zhao & Di Lorenzo, 2020).

Both northern and southern extratropical Pacific (NEP and SEP) are important to the climate variability in the tropical Pacific, albeit with distinct roles. Liguori and Di Lorenzo (2019) indicate that the NEP precursor

dynamics have a significant impact on the tropical interannual variability while the SEP precursor dynamics show no appreciable impact on ENSO. The influence of the SEP is thought to be dominant to the TPDV (Chung et al., 2019; Liguori & Di Lorenzo, 2019; Lou et al., 2019; Okumura, 2013; Sun & Okumura, 2019). However, emerging evidence suggests a mode of variability linking the North Pacific with the Central Equatorial Pacific via the NPMM at decadal timescales (Capotondi et al., 2022, 2023; Di Lorenzo et al., 2023; C. Liu et al., 2022; Newman et al., 2016).

The studies conducted thus far leave uncertainties regarding the relative importance of these precursors is, and on what frequency their influence on the tropics is more effective (i.e., interannual vs. low-frequency (sub-decadal to decadal) timescales). One important reason is that it is difficult to separate the contributions of the NEP and SEP dynamics to the tropical climate variability, since the physical interactions between extratropical Pacific and tropical Pacific occur on a wide range of spatial and temporal scales (e.g., Capotondi et al., 2023; Di Lorenzo et al., 2023; Z. Liu & Di Lorenzo, 2018; Newman et al., 2016). Many investigations address this issue using coupled climate models (e.g., Chung et al., 2019; Liguori & Di Lorenzo, 2019). However, recent studies show that significant challenges exist across models from the Coupled Model Intercomparison Project (CMIP) in reproducing the topical Pacific climate (Lyu et al., 2016; Power et al., 2021; Zhao et al., 2021b, 2023), suggesting that the relative importance of NEP and SEP dynamics may vary depending on the specific model employed.

A multivariate dynamical system—Linear Inverse Model (LIM) has proven effective in capturing characteristics of observed seasonal to decadal tropical SST variability (e.g., Penland & Matrosova, 1994; Penland & Sardeshmukh, 1995 (hereafter PS95); Newman, 2007; Newman et al., 2011). Zhao et al. (2023) developed a diagnostic approach based on LIM, enabling the explicit separation of contributions from tropical and extratropical dynamics to tropical Pacific (TP) climate variability. Following Zhao et al. (2023), we use the LIM to investigate the relative importance of NEP and SEP forcing on the tropical Pacific climate variance, including ENSO and TPDV. Furthermore, we assess interactions between extratropical and tropical Pacific in climate models from the Coupled Model Intercomparison Project Phase six (CMIP6) and compare them to observations.

2. Data and Method

2.1. Data and Indices

This study utilizes monthly mean values of sea surface temperature (SST, unit: ˚C) and sea surface height (SSH, unit: m) from the European Center for Medium-Range Weather Forecasting (ECMWF) Ocean Reanalysis System 4 (ORAS4) (Balmaseda et al., 2013) for the period spanning January 1958 to December 2015. The model data include monthly mean SST and SSH output from historical simulations (r1i1p1) of 28 CMIP6 climate models (Eyring et al., 2016). Refer to Table S1 in Supporting Information S1 for the names and classifications of these models. The period of model data is from January 1950 to December 2014. To facilitate analysis, SST and SSH fields are averaged into 2° latitude × 5° longitude grid boxes. The anomalies are derived by removing the climatology seasonal cycle. Prior to the empirical orthogonal function (EOF) analysis, each field is normalized by its domain-averaged climatological standard deviation. The externally forced trend is reduced following Penland and Matrosova (2006) and Frankignoul et al. (2017) (Text 1 in Supporting Information S1). Then the principal component (PC) time series derived from the EOF analysis are used to construct the LIM.

The ENSO index is defined as the first leading PC of SST anomalies (SSTA) within the equatorial Pacific region (10˚S−10˚N). The SSTA ENSO precursor pattern is identified using a lead correlation map between the leading PC of SSTA within the equatorial Pacific region (10˚S−10˚N) during November-the following January (NDJ) and the preceding January–March (JFM) SSTA. The geographic region of the precursor pattern is 180˚E−75˚W, 60˚S−15˚S for SEP, and 160˚E−100˚W, 10˚N−60˚N for the NEP.

2.2. Linear Inverse Model

Linear inverse modeling assumes that the evolution of the dynamical system can be represented by a linear stochastic differential equation (PS95):

$$\frac{dx}{dt} = \boldsymbol{L}x + \xi. \tag{1}$$

Here, x represents the state vector; $\boldsymbol{L}$ is the linear dynamical operator defining the evolution of x, and ξ is the white noise forcing. Following PS95, the matrix $\boldsymbol{L}$ is established by:

$$\boldsymbol{L} = \tau_0^{-1} ln\{\boldsymbol{C}(\tau_0)\,\boldsymbol{C}(0)^{-1}\}, \tag{2}$$

where $\boldsymbol{C}$ (0) and $\boldsymbol{C}$ (τ_0) are the covariance matrices and lag-covariance matrix at lag τ_0, respectively. That is, $\boldsymbol{C}$ (0) = $\langle x(t)x^T(t)\rangle$ and $\boldsymbol{C}$ (τ_0) = $\langle x\,(t+\tau_0)x^T(t)\rangle$, with τ_0 = 1 month. The spatial statistics of the white noise forcing are determined by the fluctuation-dissipation relation:

$$\boldsymbol{L}\boldsymbol{C}(0) + \boldsymbol{C}(0)\,\boldsymbol{L}^T + \boldsymbol{Q} = 0. \tag{3}$$

Here, the noise covariance matrix $\boldsymbol{Q} = \langle \xi\xi^T \rangle\, dt$.

2.3. Constructing LIM and Couple/Decoupled Extratropical Pacific

To simulate the dynamics of the coupled system involving the tropical Pacific and extratropical Pacific, Equation 1 is reformulated as:

$$\frac{dx}{dt} = \frac{d}{dt}\begin{bmatrix} x_T \\ x_N \\ x_S \end{bmatrix} = \begin{bmatrix} \boldsymbol{L_{TT}}\ \boldsymbol{L_{NT}}\ \boldsymbol{L_{ST}} \\ \boldsymbol{L_{TN}}\ \boldsymbol{L_{NN}}\ \boldsymbol{L_{SN}} \\ \boldsymbol{L_{TS}}\ \boldsymbol{L_{NS}}\ \boldsymbol{L_{SS}} \end{bmatrix} \begin{bmatrix} x_T \\ x_N \\ x_S \end{bmatrix} + \begin{bmatrix} \xi_T \\ \xi_N \\ \xi_S \end{bmatrix}, \tag{4}$$

where x_T, x_N and x_S represent the variables within the TP (10°S−10°N), NEP (14°N−60°N), and SEP (60°S−14°S), respectively. The state vector x is constructed using the corresponding PC time series of detrended data. Specifically, the Full LIM incorporates the 12 leading PCs of SST_{TP}/SST_{NEP}/SST_{SEP} and the 3 leading PCs of SSH_{TP} in the state vector. Tropical Pacific SSH is incorporated because it can improve the representation of ocean dynamics and ENSO diversity within the LIM by adding information on the ocean memory (e.g., Capotondi & Sardeshmukh, 2015; Newman et al., 2011; Shin & Newman, 2021; Zhao, Newman, et al., 2021). The chosen PCs of SST_{TP}/SSH_{TP}/SST_{NEP}/SST_{SEP} explain about 92/73/68/70 percent of the variability of their respective fields. By preserving the majority of the variability in each region and variable, the LIM is able to capture as many interactions and dynamical processes between different regions and climate modes as possible. For the problem considered in this paper, noise term ξ constrained by the noise covariance matrix $\boldsymbol{Q}$ represents the atmospheric variability and any other rapidly decorrelating nonlinearity (Newman, 2007). Note that before using the LIM for diagnosis, the validity of the linear approximation of the LIM is examined through a "tau test" (PS95) (Figure S1 and Supporting Information Text 2 in Supporting Information S1).

Equation 4 is used to identify the dynamics that are encapsulated in sub-matrices of $\boldsymbol{L}$. Specifically, $\boldsymbol{L_{TT}}$, $\boldsymbol{L_{NN}}$, and $\boldsymbol{L_{SS}}$ represent the internal processes within the TP, NEP, and SEP, respectively. $\boldsymbol{L_{NT}}$ and $\boldsymbol{L_{TN}}$ encapsulate the coupling dynamics between TP and NEP; similarly, $\boldsymbol{L_{ST}}$ and $\boldsymbol{L_{TS}}$ contain the coupling dynamics between TP and SEP; $\boldsymbol{L_{NS}}$ and $\boldsymbol{L_{SN}}$ show the coupling dynamics between NEP and SEP. In the Full LIM, the tropical Pacific dynamics are governed by the local processes ($\boldsymbol{L_{TT}}x_T$) and the impacts from NEP and SEP ($\boldsymbol{L_{NT}}x_N$ *and* $\boldsymbol{L_{ST}}x_S$):

$$\frac{dx_T}{dt} = \boldsymbol{L_{TT}}x_T + \boldsymbol{L_{NT}}x_N + \boldsymbol{L_{ST}}x_S + \xi_T. \tag{5}$$

Next, we remove all the extratropical Pacific impacts by zeroing out $\boldsymbol{L_{NT}}$ and $\boldsymbol{L_{ST}}$. Then the tropical Pacific system in this Tropical-Pacific-only LIM (TP-only LIM) is controlled only by the local dynamics (e.g., Bjerknes feedback, recharge-discharge oscillation, zonal advective feedback, thermocline feedback):

$$\frac{dx_T}{dt} = \boldsymbol{L_{TT}}x_T + \xi_T. \tag{6}$$

Similarly, we construct No-NEP LIM/No-SEP LIM by zeroing out $\boldsymbol{L_{NT}}/\boldsymbol{L_{ST}}$ in the dynamical operator $\boldsymbol{L}$ to separate the different roles of the NEP and SEP in the tropical Pacific. In the No-NEP LIM, the tropical Pacific is controlled by:

$$\frac{dx_T}{dt} = \boldsymbol{L_{TT}}x_T + \boldsymbol{L_{ST}}x_S + \xi_T. \tag{7}$$

In the No-SEP LIM, the tropical Pacific is controlled by:

$$\frac{dx_T}{dt} = \boldsymbol{L_{TT}}x_T + \boldsymbol{L_{NT}}x_N + \xi_T. \tag{8}$$

Note that the number of retained EOFs in the state vector $\boldsymbol{x}$ does not notably impact the tropical Pacific SST variance pattern in either the Full LIM or decoupled LIMs (Figure S2 and Supporting Information Text 3 in Supporting Information S1).

Equations 5–8 were integrated forward in time for 5,900 years, following the approach in Penland and Matrosova (1994) to obtain the LIM realizations of the Full LIM, TP-only LIM, No-NEP LIM, and No-SEP LIM. Subsequently, each integration was partitioned into 100 segments of 59 years, constituting ensemble members characterized by identical statistical properties as the original data but diverging due to inherent system noise. With the ensembles, the uncertainty caused by the limited length of the original timeseries when analyzing the low-frequency variability is reduced. These LIM ensembles were used to isolate the low-frequency and interannual components of the SST: the low-frequency component was obtained by applying the 6-year Zhang et al. (1997) low-pass filter to the SSTA obtained from each LIM integration, while the interannual anomalies were determined by removing the low-frequency component from the full-time series. The LIM ensembles are also used for significance testing of Figure 2 in a standard Monte Carlo approach, where the variance differences between each ensemble member and the ensemble mean were used to determine the range of statistical significance.

We next constructed LIMs based on the output of each CMIP6 model, replicating the observational LIM analysis.

3. The Different Roles of NEP and SEP in Observations

3.1. Changes in ENSO Behavior Induced by Extra-Tropical Forcing

We first explore how the southern and northern extratropical dynamics impact the behavior of ENSO. The leading EOF patterns of tropical Pacific SSTA (Unit: °C) and SSH anomalies (SSHA, Unit: m) from ensembles derived from the Full LIM, TP-only LIM, No-NEP LIM, and No-SEP LIM are shown in Figures 1a–1d. All patterns align with the canonical ENSO pattern, characterized by the largest SSTA occurring in the central and eastern Pacific and extending to the eastern ocean boundary. When the extratropical Pacific is fully decoupled (TP-only LIM), the leading SSTA/SSHA pattern (Figure 1b) exhibits substantially weaker amplitude and is more confined to the equatorial Pacific region compared to the Full LIM (Figure 1a). In the No-NEP LIM, dominant patterns are akin to those in the Full LIM (Figure 1c vs. Figure 1a), but with weaker amplitude in the central Pacific region. The removal of only the SEP impacts on the TP strongly weakens the amplitude of the leading mode, especially in the eastern tropical Pacific (Figure 1d vs. Figure 1a). This indicates that NEP/SEP dynamics are primarily responsible for weaker ENSO amplitude in the central/eastern tropical Pacific region seen in the TP-only LIM (Figure 1a).

The associated variance of the leading SST EOF (the plus signs in Figure 1f) reveals a substantial 46% reduction in the TP-only LIM and No-SEP LIM and a 22% decrease in the No-NEP LIM, compared to the variance in the Full LIM. This suggests that the SEP dynamics play a more important role in driving the ENSO variance.

The power spectra of the ENSO index are examined to investigate the extratropical impact on the temporal features of ENSO. The mean spectrum from the Full LIM ensemble (Figure 1e, red line) exhibits a commendable agreement with the observational spectrum (Figure 1e, blue line), with maximum power at timescales of ∼3 years, indicating that the Full LIM can reproduce the temporal characteristics of the dominant tropical Pacific SSTA mode. By contrast, fully decoupling the extratropical Pacific significantly reduces the variance of the ENSO mode at periods larger than 2 years and tends to shorten the dominant timescale of the leading PC to 2 years (Figure 1e, orange line). ENSO spectrum in No-NEP LIM (Figure 1e, dashed green line) exhibits a reduction in the period

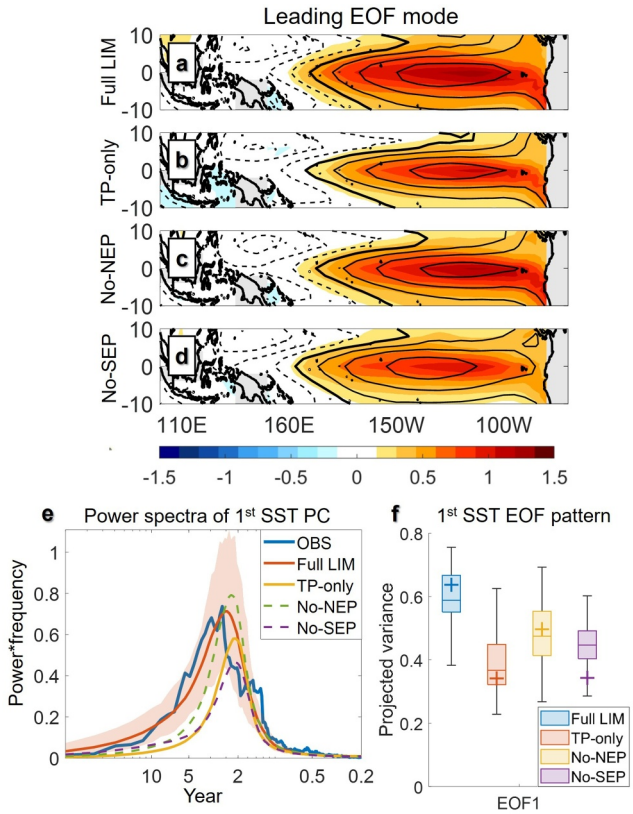

Figure 1. Leading SST (shading) and SSH (contours, negative values dashed) EOF patterns of the tropical Pacific in (a) Full LIM, (b) TP-only LIM, (c) No-NEP LIM, and (d) No-SEP LIM. The unit of the SSTA is °C. The contour interval of SSHA is 0.02 m. (e) Power spectra of leading tropical Pacific SST PC in observation (blue line), Full LIM (red line), TP-only LIM (orange line), No-NEP LIM (dashed purple line), and No-SEP LIM (dashed green line). The power spectra of the LIMs show the mean of the spectra from the 100 members of the LIM ensembles. The pink shading shows the 90% confidence interval determined from the 100 samples of the Full LIM. (f) The summary statistics for the variance of the dominant SST EOF of the various LIM ensembles in different CMIP6 models. The variances are normalized by the total variance of the original tropical Pacific SSTAs. The plus signs show the results of observation. Lines inside the boxes show the sample median. The top and bottom edges of each box are the upper and lower quartiles, respectively.

larger than 3 years compared to the Full LIM, while it slightly increases in timescales of ~2 years, leading to a peak power at 2 years. The overall power of the No-SEP LIM is similar to that of the TP-only LIM (Figure 1e, the dashed purple line and the orange line), but with even weaker power at ~2 years. It is also worth noting that the low-frequency power of ENSO is reduced at different levels in the simulations of all the decoupled LIMs (Figure 1e).

ENSO events typically exhibit a diversity of spatial patterns, categorized into eastern-Pacific (EP) and central-Pacific (CP) types, as elucidated by Capotondi et al. (2015). We identify EP-ENSO and CP-ENSO following Takahashi et al. (2011), and find that the changes in spatial-temporal characteristics of different types of ENSO when decoupling the extratropical Pacific (Figure S3 in Supporting Information S1) closely resemble the changes observed in the leading SST EOF mode.

Thus, both the spatial pattern and variance of ENSO are influenced by the extratropical Pacific. Furthermore, the NEP and SEP appear to play distinctive roles in shaping the interannual and low-frequency variance within the tropical Pacific, topics that will be expounded upon in detail in the subsequent section.

3.2. Extra-Tropical Forcing of Tropical Interannual and Low-Frequency Variability

To evaluate the overall impact of the NEP and SEP dynamics on tropical Pacific interannual variability, we compare the SST interannual variance pattern of the Full LIM and the decoupled LIMs (Figures 2a–2d). The full interannual SST variance has the largest amplitude in the cold tongue region, extending westward with diminishing amplitude (Figure 2a). Removing the extratropical impacts leads to a decoupled SST variance (Figure 2b) that is substantially reduced, especially in the east of the dateline (~40%) (Figure 2e). A similar scenario unfolds when only the impacts of the SEP are removed (Figures 2d and 2g vs. Figures 2b and 2e). In contrast, if only the impacts of the NEP are removed, the interannual SST variance remains practically unchanged (Figure 2c vs. Figure 2a, see also Figure 2f). This suggests that SEP dynamics exert important impacts on the tropical interannual SST variance, especially in the eastern part of the basin (Figure 2g), while the NEP influence seems to be small (Figure 2f). This is consistent with T. Liu et al. (2024), in which they found the impacts from the SEP on ENSO are stronger than those from the NEP by applying the regional data assimilation approach in a coupled climate model.

The impact of extratropical dynamics on tropical Pacific SST anomalies is even more pronounced for low-frequency variability. In the Full LIM, the low-frequency SST variance (Figure 2h) exhibits a broader meridional scale than the variance at interannual timescales (Figure 2a), with the largest values located in the central equatorial Pacific (near the dateline) rather than in the eastern part of the basin, as typical of ENSO anomalies (Figure 2a). In comparison to the Full LIM, TP-only low-frequency variance (Figure 2i) is significantly reduced by more than 70% in most regions of the tropical Pacific (Figure 2l), suggesting that extratropical dynamics explain the largest fraction of the tropical Pacific low-frequency SST, consistent to previous studies (Zhao & Di Lorenzo, 2020; Zhao et al., 2023). The removal of the NEP coupling in the No-NEP LIM results in a statistically significant decrease of low-pass filtered variance in the central tropical Pacific (Figures 2i and 2m), where decadal SST variability associated with the NPMM typically occurs (Capotondi et al., 2022; Di Lorenzo et al., 2023; C. Liu et al., 2022; Newman et al., 2016). In contrast, when only removing the SEP dynamics, the No-SEP low-frequency variance significantly decreases in the southeastern tropical Pacific region, where SST variability linked to the SPMM (Zhang et al., 2014) typically occurs (Figure 2n).

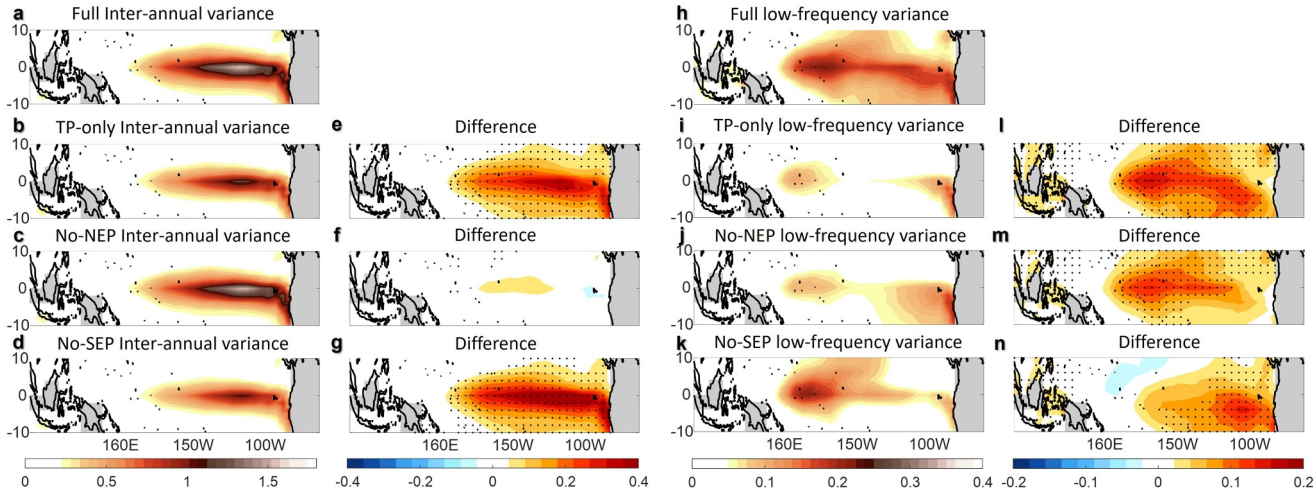

Figure 2. SST ensemble-mean interannual variance patterns ($^{\circ}C^2$) in (a) Full LIM, (b) TP-only LIM, (c) No-NEP LIM, and (d) No-SEP LIM. Difference between interannual SST variance of Full LIM and (e) TP-only SST inter-annual variance, (f) No-NEP SST inter-annual variance, and (g) No-SEP inter-annual variance (h–n) Similar to (a)–(g) but for the SST ensemble-mean low-frequency variance patterns ($^{\circ}C^2$). The interannual SST anomalies are obtained by removing the 6-year lowpass anomalies from the LIM time series and then are used to calculate the interannual variance. The 6-year lowpass SST anomalies are used to calculate the low-frequency variance. Black dots show the differences exceeding the 90% significant level obtained from the variance differences of each of the 100 samples with the ensemble mean of the corresponding LIMs. Note that similar results were obtained when using the 8-year lowpass filter (figures not shown).

The extratropical dynamics also significantly change the dominant mode of the tropical Pacific low-frequency variability (Figure S4 in Supporting Information S1). In the Full LIM, the leading low-frequency EOF of SSTAs (Figure S4a in Supporting Information S1) depicts the well-known ENSO-like TPDV pattern (Capotondi et al., 2023; Power et al., 2021; Zhang et al., 1997). The second leading low-frequency SSTA EOF (Figure S4e in Supporting Information S1) displays a zonal dipole pattern, with a maximum in the warm pool region and an opposite-polarity anomaly of roughly equal amplitude in the eastern tropical Pacific. After decoupling the extratropical Pacific, the leading SSTA mode becomes a zonal dipole pattern (Figure S4b in Supporting Information S1), resembling the second dominant mode in the Full LIM (Fig. S4e in Supporting Information S1), while the TPDV becomes the second leading mode (Figure S4f in Supporting Information S1). This suggests that the TPDV mode (Figure S4a in Supporting Information S1) is mainly driven by extratropical dynamics, aligning with the findings of Zhao and Di Lorenzo (2020) that extratropical precursor dynamics explain the largest fraction of TPDV. However, the second low-frequency SSTA mode (Figure S4e in Supporting Information S1) is mostly induced by the local tropical dynamics (e.g., ENSO residuals), consistent with Kim and Kug (2020)'s results that this zonal dipole decadal variability largely originates from the decadal modulation of ENSO amplitude and asymmetry.

In the No-NEP(No-SEP) LIM, the dominant low-frequency SSTA EOF exhibits an EP-ENSO-like (CP-ENSO-like) pattern (Figures S4c–S4d in Supporting Information S1), while the second dominant SSTA EOF closely resembles the CP-ENSO (EP-ENSO) pattern (Figures S4g–S4h in Supporting Information S1). These findings align with the alterations observed in the low-frequency SST variance (Figures 2h–2n), highlighting the distinct tropical Pacific regions influenced by the NEP and SEP dynamics in shaping low-frequency variance.

4. Examine the Behaviors of CMIP6 Models

In this section, we use the LIM model to evaluate 28 climate models from CMIP6 (Table S1 in Supporting Information S1) to assess their ability to replicate observed impacts of the NEP/SEP on TP climate viability.

We first examine the impacts of NEP/SEP on ENSO in CMIP6 models. Decoupling the extratropical Pacific or selectively removing the NEP/SEP impacts does not notably change the pattern of the leading SSTA EOF, CP-ENSO, and EP-ENSO (Figures S5 in Supporting Information S1). This suggests a prevailing tendency among models to underestimate the impact of the extratropical Pacific on the ENSO pattern.

The boxes in Figure 1f show the summary statistic for the variance of the SST dominant mode in different CMIP6 models, revealing large spreads among models in both the Full LIM and the decoupled LIMs. In the coupled

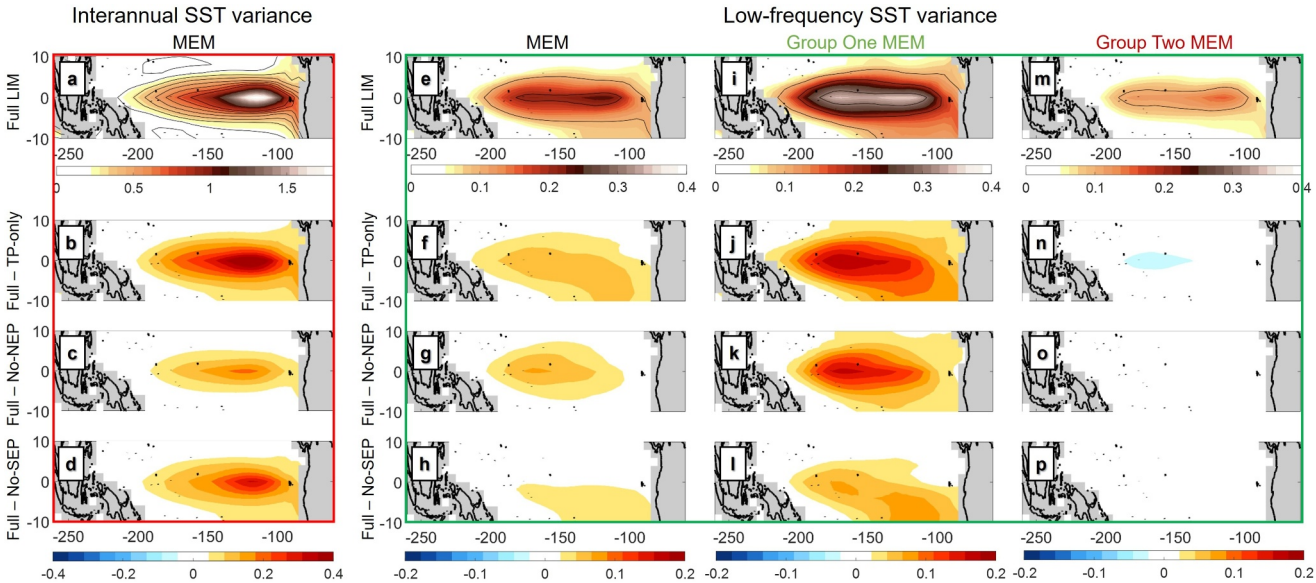

Figure 3. (a) Tropical Pacific interannual SST variance patterns (°C^2) of CMIP6 MEM. Difference between MEM Full LIM interannual SST variance and (b) MEM TP-only SST variance, (c) MEM No-NEP SST variance, and (d) MEM No-SEP variance. (e) Tropical Pacific low-frequency SST variance patterns (°C^2) of CMIP6 MEM. Difference between MEM Full LIM low-frequency SST variance and (f) MEM TP-only SST variance, (g) MEM No-NEP SST variance, and (h) MEM No-SEP variance (i–l) Similar to (e)–(h) but for Group One MEM (m–p) Similar to (e)–(h) but for Group Two MEM.

system (Full LIM), most models (>50%) underestimate the observed variance of the dominant SST mode (blue box and blue plus in Figure 1f). Fully decoupling the extratropical Pacific (TP-only LIM) results in a significant decrease in ENSO variance compared to the Full LIM in CMIP6 models (red box vs. blue box in Figure 1f). However, most models (>50%) overestimate the observed TP-only ENSO variance, suggesting the impacts of extratropical Pacific on ENSO variance are generally weaker in most CMIP6 models. When only removing the impacts of the NEP (yellow box in Figure 1f), the No-NEP ENSO variance decreases compared to the Full LIM (blue box in Figure 1f) but remains larger than the TP-only variance (red box in Figure 1f), aligning with observations (the plus signs in Figure 1f). In the No-SEP LIM, most models (>75%) largely overestimate the observed No-SEP ENSO variance (purple box and purple plus in Figure 1f), indicating a widespread underestimation of the impacts of SEP dynamics on ENSO variance in CMIP6 models.

Note that the summary statistics for the variance of the EP-ENSO and CP-ENSO patterns in different CMIP6 models (Figure S3j in Supporting Information S1) parallel those for the variance of the dominant SST mode (Figure 1f). Therefore, the impacts of the extratropical Pacific, especially the SEP, on ENSO variance (including EP-ENSO and CP-ENSO) are largely underestimated in most CMIP6 models.

We then examine the impacts of the extratropical Pacific on the tropical Pacific interannual variance in CMIP6 models (first column in Figure 3). The MEM interannual SST variance demonstrates similarity to observations, but with stronger variability in the eastern tropical Pacific (Figure 3a vs. Figure 2a). When decoupling the extratropical Pacific, the TP-only variance decreases (Figure 3b), although the extent of the variance reduction (∼30%) is somewhat smaller than observed (∼40%). When only removing the NEP impacts, the interannual SST variance does not change much (Figure 3c), aligning with the observations (Figure 2f). The No-SEP interannual SST variability also exhibits a reduced amplitude compared to the Full LIM (Figure 3d), again, the contribution of the SEP is notably underestimated in the models (∼20% in the MEM vs. ∼40% in the observations). After inspecting the interannual variance of each CMIP6 model (Figures S6–S9 in Supporting Information S1), it becomes evident that the MEM effectively captures the behavior of most models.

Furthermore, we examine the representation of the tropical Pacific low-frequency SST variance in CMIP6 models, revealing a substantial spread across models and significant deviations from observations, in line with findings by Zhao et al. (2023) (Figure S10 in Supporting Information S1). This emphasizes the need for cautious interpretation when evaluating low-frequency variance. For the MEM, the low-frequency SST variance of the Full LIM exhibits heightened intensity in the eastern tropical Pacific (Figure 3e) compared to observations

(Figure 2h). In the decoupled LIMs, the MEM low-frequency SST variance remains relatively unchanged in comparison to the Full LIM (Figures 3f–3h), a contrast to observations. However, in the full suite of CMIP6 models, the changes in the low-frequency variance when decoupling the extratropical Pacific display considerable variability among models (Figure S11 in Supporting Information S1). In some models (e.g., CESM2-WACCM, CMCC-ESM2, MIROC6), the TP-only low-frequency variance experiences a notable reduction, aligning with observations. In contrast, some models show nearly unchanged (e.g., FGOALS-g3, GFDL-CM4) or even increased (e.g., UKESM1-0-LL) TP-only low-frequency variance when compared to the Full LIM (Figure S11 in Supporting Information S1). To delve deeper into the low-frequency variance in CMIP6 models, we classify the models into two groups according to the differences between the total low-frequency SST variance and the TP-only low-frequency SST variance within 10°S–10°N. Models exhibiting a positive spatial mean difference larger than 0.01 ($°C^2$) are classified into Group One, while others are categorized into Group Two (Table S1 in Supporting Information S1).

Generally, the total low-frequency variance is much stronger in Group One MEM than that in Group Two MEM (Figure 3i vs. Figure 3m). In Group One models, extratropical dynamics make a significant positive contribution to the overall low-frequency variance (∼50%–60%), although this is smaller than observed (>70%). The NEP (SEP) mainly contributes to low-frequency variance in the central (southeastern) tropical Pacific region (Figs. k–l), aligning with the observations (Figures 2m and 2n). However, Group One models tend to substantially underestimate the observed SEP contribution (Figure 2n vs. Figure 3l). This suggests that, in general, the tropical Pacific low-frequency variability is considerably impacted by extratropical Pacific dynamics in Group One models, although the impacts are less pronounced than observed, especially in terms of SEP impacts. While in Group Two models, the overall contribution of the extratropical Pacific (including both the NEP and SEP dynamics) is minimal (Figures 3n–3p).

Given the established significance of extratropical ENSO precursor dynamics in influencing tropical Pacific climate variability (e.g., Alexander et al., 2010; Di Lorenzo et al., 2015; Thomas & Vimont, 2016; You & Furtado, 2017; Zhao & Di Lorenzo, 2020), we examine the representation of the SSTA ENSO precursor pattern (see Method Section 2.1) in CMIP6 models. The observed SSTA precursor pattern (Figure 4a) is characterized by the typical footprinting pattern (Vimont et al., 2001, 2003a, 2003b) and shares common features with the NPMM (Chiang & Vimont, 2004) in the North Pacific, and resemble the typical pattern of the SPMM (Zhang et al., 2014) in the South Pacific. Group One models can better reproduce the extratropical SSTA precursor pattern, especially the footprinting pattern in the North Pacific (Figures 4c and 4d). The spatial correlation coefficient (SCC) of the NEP ENSO precursor pattern between observations and models is larger than 0.5 in 9 of 12 Group One models (green asterisks in Figure 4f), while the SCC in most Group Two models is smaller than 0.5 (red asterisks in Figure 4f).

We next examine the power spectrum of the ENSO index in CMIP6 models, revealing substantial variability among the power spectra in different climate models (light green and red lines in Figure 4e). Nevertheless, the ensemble mean power spectrum, averaged across models with drastically different power spectra, closely resembles the observed (blue line vs. black line in Figure 4e), exhibiting maximum power at timescales of approximately 3 years. However, the models tend to underestimate the decadal power of the ENSO (>10 years). The Group One MEM power spectrum shows much more power at longer timescales (>3 years) than the Group Two MEM, featuring a prominent peak at longer time scales (3–4 years) in contrast to the Group Two MEM (2.5–3 years) (green line and red line in Figure 4e).

In observations, the low-frequency tropical variance (>6 years) to total tropical variance ratio is about 0.36 (the gray line on the right in Figure 4g), while CMIP6 models exhibit a wider range from 0.05 to 0.47 (x-axis in Figures 4f and 4g), in which 26 out of 28 models underestimate the ratio. Our analysis reveals that CMIP6 models with enhanced low (high) frequency ENSO power are associated with stronger NEP (SEP) dynamics. Specifically, models exhibiting a better representation of the NEP ENSO precursor tend to manifest ENSO behaviors with more low-frequency variability (>6 years). This is evident from the strong correlation (0.6) between the fractions of the low-frequency power of the ENSO index and the SCCs of the NEP precursor pattern in CMIP6 models (Figure 4f). This implies that the NEP ENSO precursor dynamics play a crucial role in shaping the low-frequency variance while having a limited impact on the interannual variance, aligning with the observations presented in Figure 2. Conversely, the negative correlation (−0.53) between the SCCs of the SEP precursor pattern and the fraction of low-frequency power (>6 years) of the ENSO in CMIP6 models (Figure 4g) implies

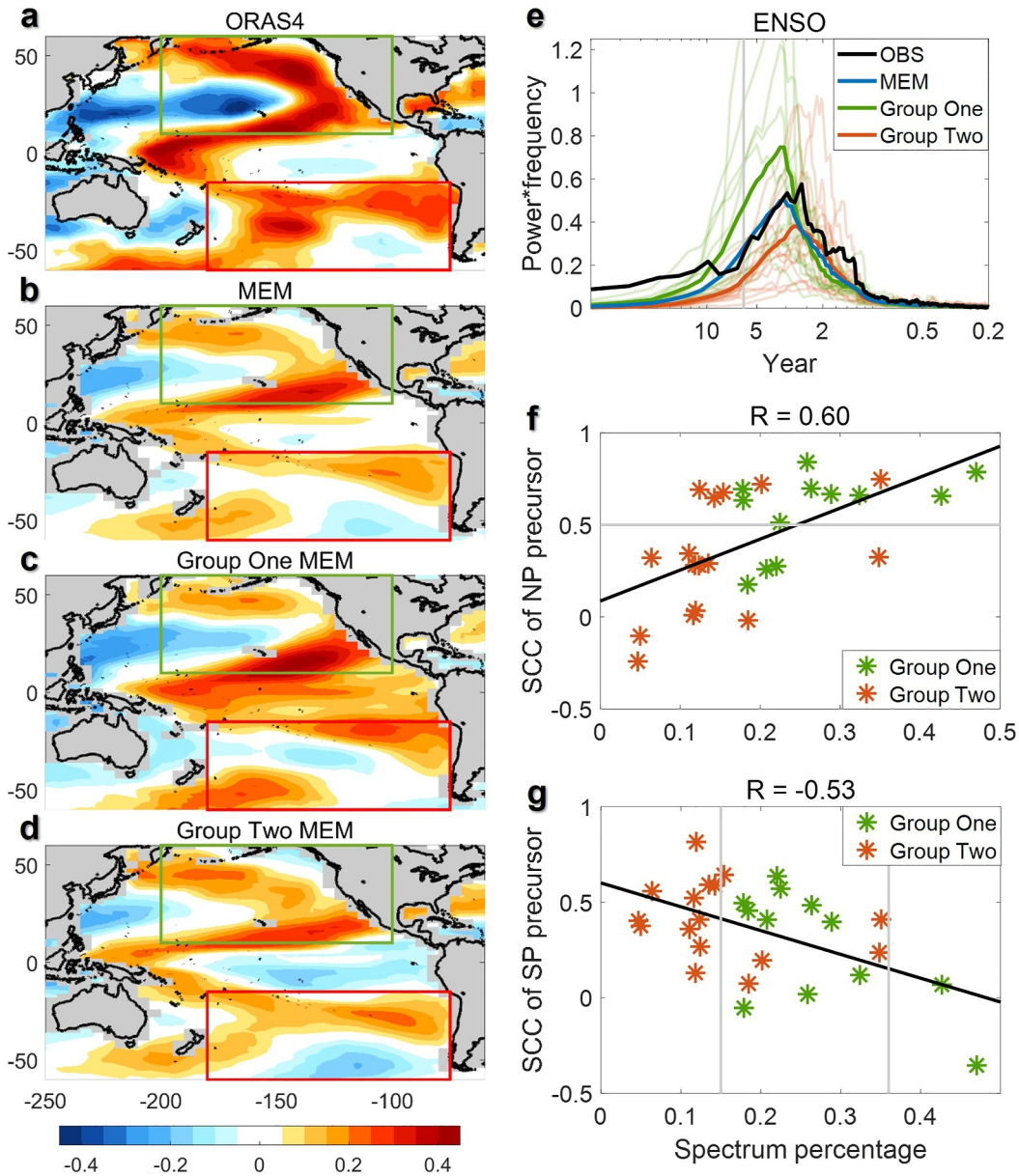

Figure 4. Extra-tropical ENSO precursor pattern of (a) ORAS4, (b) CMIP6 MEM, (c) Group One MEM, and (d) Group Two MEM. (e) Power spectra of ENSO index of observations (black line), CMIP6 MEM (blue line), Group One MEM (green line), and Group Two MEM (red line). ENSO index is defined as the leading PC of the tropical Pacific SST. The spectra of Group One (Two) models are shown in light green (red) lines. (f) The *x*-axis shows the fraction of the low-frequency power (>6 years) to the total power of the ENSO index in each CMIP6 model. The *y*-axis shows the spatial correlation coefficient of the North Pacific precursor pattern between each CMIP6 model and observation. (g) Similar to (f), but the *y*-axis shows the spatial correlation coefficient of the South Pacific precursor pattern between each CMIP6 model and observation. Group One (Two) models are shown in green (red) points.

that models that can better simulate the SEP ENSO precursors tend to exhibit ENSO with more interannual variance. This aligns with the observed substantial reduction in interannual variance, which is much larger than the reduction in low-frequency variance in the absence of the SEP (Figure 2g vs. Figure 2n).

5. Summary and Discussion

Using an empirical dynamical model (LIM) that allowed us to selectively include or exclude the NEP or SEP coupling linked to the ENSO precursors, we explore the different roles of the NEP and SEP in the tropical Pacific

interannual and low-frequency (sub-decadal to decadal) variability. We find that both NEP and SEP dynamics energize the tropical variance independently on different timescales. Specifically, SEP dynamics significantly contribute to the tropical Pacific interannual variance (~40%) and the low-frequency variance in the southeastern tropical Pacific (~70%), while the absence of the NEP dynamics has negligible impact on interannual variance, but substantially reduces low-frequency variance in the central tropical Pacific (~70%) (Figure 2). It is worth mention that some trans-basin influence may be also implicitly included in the LIM. For example, the Atlantic climate modes may impact the NPMM through atmospheric teleconnection (e.g., Ham et al., 2013; Ma et al., 2021). However, it is likely to be secondary compared to the internal interactions within the Pacific.

Moreover, CMIP6 climate models exhibiting a better representation of extratropical contributions to TP low-frequency variance (Group One models) also tend to more accurately simulate the NEP ENSO precursor pattern and manifest ENSO with more low-frequency power (Figures 4a–4e). Additionally, there exists a correlation between the models' proficiency in representing extratropical ENSO precursor patterns and ENSO spectral characteristics. Specifically, CMIP6 models that better simulate NEP (SEP) extratropical ENSO precursor patterns are typically associated with ENSO behaviors featuring more low-frequency (high-frequency) variance (Figures 4f and 4g).

Analysis of CMIP6 models reveals a widespread underestimation of the impacts of the extratropical Pacific, especially the SEP, on ENSO variance (including EP-ENSO and CP-ENSO) (Figure 1f) and the TP interannual variance (first column in Figure 3). Many models (16 of 28, Group Two) fail to reproduce the contribution of extratropical Pacific (including the NEP and SEP) to TP low-frequency variance, while other models (12 of 28, Group One) exhibit an underestimation of this contribution, especially concerning the SEP (Figure 3). Zhao, Di Lorenzo, et al. (2021) examined the tropical Pacific decadal variability and its connection to extratropical dynamics in CMIP5 models using statistical methods. Although using different methods, the revealed model biases of CMIP5 models are consistent with those of the CMIP6 models shown in this work. That is, most CMIP5 models underestimate the impacts of the extratropical Pacific ENSO precursors on the tropical Pacific climate variability. In line with the findings of Zhao, Di Lorenzo, et al. (2021), which indicated that models with a more accurate representation of ENSO precursors tend to better simulate basin-scale signatures of TPDV and exhibit stronger ENSO teleconnections consistent with observations, this study also emphasizes the importance of enhancing the simulation of tropical-extratropical interactions, particularly those involving the SEP, in climate models, to improve the understanding and predictability of tropical Pacific climate variability.

Data Availability Statement

The ORAS4 output can be downloaded from: https://www.cen.uni-hamburg.de/en/icdc/data/ocean/easy-init-ocean/ecmwf-ocean-reanalysis-system-4-oras4.html. The CMIP6 models used in this work are listed in Table S1 in Supporting Information S1. The model data were obtained from https://esgf-node.llnl.gov/projects/cmip6/.

Acknowledgments
This work is supported by the National Natural Science Foundation of China (42206210 to D. S., and 42206025 to Y. Z.), and the Taishan Scholars Program (No. tsqn202306298 to D. S., and No. tsqn202306299 to Y. Z.). E. D. L. is supported by the U.S. Department of Energy's Regional and Global Model Analysis program (No. DE-SC0023228).

References

Alexander, M. A., Bladé, I., Newman, M., Lanzante, J. R., Lau, N.-C., & Scott, J. D. (2002). The atmospheric bridge: The influence of ENSO teleconnections on air–sea interaction over the global oceans. *Journal of Climate*, *15*(16), 2205–2231. https://doi.org/10.1175/1520-0442(2002)015<2205:tabtio>2.0.co;2

Alexander, M. A., Vimont, D. J., Chang, P., & Scott, J. D. (2010). The impact of extratropical atmospheric variability on ENSO: Testing the seasonal footprinting mechanism using coupled model experiments. *Journal of Climate*, *23*(11), 2885–2901. https://doi.org/10.1175/2010JCLI3205.1

Anderson, B. T. (2003). Tropical Pacific sea-surface temperatures and preceding sea level pressure anomalies in the subtropical North Pacific. *Journal of Geophysical Research*, *108*, 4732. https://doi.org/10.1029/2003JD003805

Anderson, B. T., Perez, R. C., & Karspeck, A. (2013). Triggering of El Nino onset through trade wind-induced charging of the equatorial Pacific. *Geophysical Research Letters*, *40*(6), 1212–1216. https://doi.org/10.1002/grl.50200

Balmaseda, M. A., Mogensen, K., & Weaver, A. T. (2013). Evaluation of the ECMWF ocean reanalysis system ORAS4. *Quarterly Journal of the Royal Meteorological Society*, *139*(674), 1132–1161. https://doi.org/10.1002/qj.2063

Capotondi, A., McGregor, S., McPhaden, M. J., Cravatte, S., Holbrook, N. J., Imada, Y., et al. (2023). Mechanisms of tropical Pacific decadal variability. *Nature Reviews Earth & Environment*, *4*(11), 754–769. https://doi.org/10.1038/s43017-023-00486-x

Capotondi, A., Newman, M., Xu, T., & Di Lorenzo, E. (2022). An optimal precursor of Northeast Pacific marine heatwaves and central Pacific El Niño events. *Geophysical Research Letters*, *49*(5), e2021GL097350. https://doi.org/10.1029/2021gl097350

Capotondi, A., & Sardeshmukh, P. D. (2015). Optimal precursors of different types of ENSO events. *Geophysical Research Letters*, *42*(22), 9952–9960. https://doi.org/10.1002/2015gl066171

Capotondi, A., Wittenberg, A. T., Kug, J. S., Takahashi, K., & McPhaden, M. J. (2020). ENSO diversity. El Niño southern oscillation in a changing climate. *Geophysical Monograph Series*, *253*, 65–86.

Capotondi, A., Wittenberg, A. T., Newman, M., Di Lorenzo, E., Yu, J. Y., Braconnot, P., et al. (2015). Understanding ENSO diversity. *Bulletin of the American Meteorological Society*, *96*(6), 921–938. https://doi.org/10.1175/bams-d-13-00117.1

Chang, P., Zhang, L., Saravanan, R., Vimont, D. J., Chiang, J. C. H., Ji, L., et al. (2007). Pacific meridional mode and El Niño–southern oscillation. *Geophysical Research Letters*, *34*(16), L16608. https://doi.org/10.1029/2007gl030302

Chiang, J. C. H., & Vimont, D. J. (2004). Analogous Pacific and Atlantic meridional modes of tropical atmosphere–ocean variability. *Journal of Climate*, *17*(21), 4143–4158. https://doi.org/10.1175/jcli4953.1

Chung, C. T. Y., Power, S. B., Sullivan, A., & Delage, F. (2019). The role of the South Pacific in modulating tropical Pacific variability. *Scientific Reports*, *9*(1), 18311. https://doi.org/10.1038/s41598-019-52805-2

Di Lorenzo, E., Combes, V., Keister, J., Strub, P. T., Thomas, A., Franks, P., et al. (2013). Synthesis of Pacific Ocean climate and ecosystem dynamics. *Oceanography*, *26*(4), 68–81. https://doi.org/10.5670/oceanog.2013.76

Di Lorenzo, E., Liguori, G., Schneider, N., Furtado, J. C., Anderson, B. T., & Alexander, M. A. (2015). ENSO and meridional modes: A null hypothesis for Pacific climate variability. *Geophysical Research Letters*, *42*(21), 9440–9448. https://doi.org/10.1002/2015GL066281

Di Lorenzo, E., Xu, T., Zhao, Y., Newman, M., Capotondi, A., Stevenson, S., et al. (2023). Modes and mechanisms of Pacific decadal-scale variability. *Annual Review of Marine Science*, *15*(1), 249–275. https://doi.org/10.1146/annurev-marine-040422-084555

Eyring, V., Bony, S., Meehl, G. A., Senior, C. A., Stevens, B., Stouffer, R. J., & Taylor, K. E. (2016). Overview of the coupled model Intercomparison Project Phase 6 (CMIP6) experimental design and organization. *Geoscientific Model Development*, *9*(5), 1937–1958. https://doi.org/10.5194/gmd-9-1937-2016

Fisman, D. N., Tuite, A. R., & Brown, K. A. (2016). Impact of El Nino southern oscillation on infectious disease hospitalization risk in the United States. *P. Natl. Acad. Sci. USA*, *113*(51), 14589–14594. https://doi.org/10.1073/pnas.1604980113

Frankignoul, C., Gastineau, G., & Kwon, Y. O. (2017). Estimation of the SST response to anthropogenic and external forcing and its impact on the Atlantic multidecadal oscillation and the Pacific decadal oscillation. *Journal of Climate*, *30*(24), 9871–9895. https://doi.org/10.1175/jcli-d-17-0009.1

Ham, Y.-G., Kug, J.-S., Park, J.-Y., & Jin, F.-F. (2013). Sea surface temperature in the north tropical Atlantic as a trigger for El Niño/Southern Oscillation events. *Nature Geoscience*, *6*(2), 112–116. https://doi.org/10.1038/NGEO1686

Kim, G., & Kug, J. (2020). Tropical Pacific decadal variability induced by nonlinear rectification of El Niño–southern oscillation. *Journal of Climate*, *33*(17), 7289–7302. https://doi.org/10.1175/jcli-d-19-0123.1

Larson, S., & Kirtman, B. (2013). The Pacific Meridional Mode as a trigger for ENSO in a high-resolution coupled model. *Geophysical Research Letters*, *40*(12), 3189–3194. https://doi.org/10.1002/grl.50571

Larson, S., & Kirtman, B. (2014). The Pacific Meridional Mode as an ENSO precursor and predictor in the North American multimodel ensemble. *Journal of Climate*, *27*(18), 7018–7032. https://doi.org/10.1175/JCLI-D-14-00055.1

Liguori, G., & Di Lorenzo, E. (2018). Meridional modes and increasing Pacific decadal variability under anthropogenic forcing. *Geophysical Research Letters*, *45*(2), 983–991. https://doi.org/10.1002/2017GL076548

Liguori, G., & Di Lorenzo, E. (2019). Separating the North and South Pacific meridional modes contributions to ENSO and tropical decadal variability. *Geophysical Research Letters*, *46*(2), 906–915. https://doi.org/10.1029/2018GL080320

Liu, C., Zhang, W., Jin, F.-F., Stuecker, M. F., & Geng, L. (2022). Equatorial origin of the observed tropical Pacific quasi-decadal variability from ENSO nonlinearity. *Geophysical Research Letters*, *49*(10), e2022GL097903. https://doi.org/10.1029/2022gl097903

Liu, T., Liu, Z., Zhao, Y., & Zhang, S. (2024). Strong extratropical impact on observed ENSO. *Journal of Climate*, *37*(3), 943–962. https://doi.org/10.1175/jcli-d-23-0023.1

Liu, Z., & Di Lorenzo, E. (2018). Mechanisms and predictability of Pacific decadal variability. *Current Climate Change Reports*, *4*(2), 128–144. https://doi.org/10.1007/s40641-018-0090-5

Lou, J., Holbrook, N. J., & O'Kane, T. J. (2019). South Pacific decadal climate variability and potential predictability. *Journal of Climate*, *32*(18), 6051–6069. https://doi.org/10.1175/jcli-d-18-0249.1

Lyu, K., Zhang, X., Church, J. A., & Hu, J. (2016). Evaluation of the interdecadal variability of sea surface temperature and sea level in the Pacific in CMIP3 and CMIP5 models. *International Journal of Climatology*, *36*(11), 3723–3740. https://doi.org/10.1002/joc.4587

Ma, J., Xie, S.-P., Xu, H., Zhao, J., & Zhang, L. (2021). Cross-basin interactions between the tropical Atlantic and Pacific in the ECMWF hindcasts. *Journal of Climate*, *34*(7), 2459–2472. https://doi.org/10.1175/JCLI-D-20-0140.1

Newman, M. (2007). Interannual to decadal predictability of tropical and North Pacific sea surface temperatures. *Journal of Climate*, *20*(11), 2333–2356. https://doi.org/10.1175/JCLI4165.1

Newman, M., Alexander, M. A., Ault, T. R., Cobb, K. M., Deser, C., Di Lorenzo, E., et al. (2016). The Pacific decadal oscillation, revisited. *Journal of Climate*, *29*(12), 4399–4427. https://doi.org/10.1175/JCLI-D-15-0508.1

Newman, M., Alexander, M. A., & Scott, J. D. (2011). An empirical model of tropical ocean dynamics. *Climate Dynamics*, *37*(9–10), 1823–1841. https://doi.org/10.1007/s00382-011-1034-0

Okumura, Y. M. (2013). Origins of tropical Pacific decadal variability: Role of stochastic atmospheric forcing from the South Pacific. *Journal of Climate*, *26*(24), 9791–9796. https://doi.org/10.1175/jcli-d-13-00448.1

Penland, C., & Matrosova, L. (1994). A balance condition for stochastic numerical models with application to the El Nino-Southern Oscillation. *Journal of Climate*, *7*(9), 1352–1372. https://doi.org/10.1175/1520-0442(1994)007<1352:abcfsn>2.0.co;2

Penland, C., & Matrosova, L. (2006). Studies of El Niño and interdecadal variability in tropical sea surface temperatures using a nonnormal filter. *Journal of Climate*, *19*(22), 5796–5815. https://doi.org/10.1175/JCLI3951.1

Penland, C., & Sardeshmukh, P. D. (1995). The optimal-growth of tropical sea-surface temperature anomalies. *Journal of Climate*, *8*(8), 1999–2024. https://doi.org/10.1175/1520-0442(1995)008<1999:togots>2.0.co;2

Power, S., Lengaigne, M., Capotondi, A., Khodri, M., Vialard, J., Jebri, B., et al. (2021). Decadal climate variability in the tropical Pacific: Characteristics, causes, predictability, and prospects. *Science*, *374*(6563), eaay9165. https://doi.org/10.1126/science.aay9165

Shin, S.-I., & Newman, M. (2021). Seasonal Predictability of global and North American coastal sea surface temperature and height anomalies. *Geophysical Research Letters*, *48*(10), e2020GL091886. https://doi.org/10.1029/2020GL091886

Sun, T., & Okumura, Y. M. (2019). Role of stochastic atmospheric forcing from the South and North Pacific in tropical Pacific decadal variability. *Journal of Climate*, *32*(13), 4013–4038. https://doi.org/10.1175/jcli-d-18-0536.1

Takahashi, K., Montecinos, A., Goubanova, K., & Dewitte, B. (2011). ENSO regimes: Reinterpreting the canonical and Modoki El Niño. *Geophysical Research Letters*, *38*(10), L10704. https://doi.org/10.1029/2011GL047364

Thomas, E. E., & Vimont, D. J. (2016). Modeling the mechanisms of linear and nonlinear ENSO responses to the Pacific Meridional Mode. *Journal of Climate*, *29*(24), 8745–8761. https://doi.org/10.1175/JCLI-D-16-0090.1

Vimont, D., Battisti, D., & Hirst, A. (2003). The seasonal footprinting mechanism in the CSIRO general circulation models. *Journal of Climate*, *16*, 2653–2667. https://doi.org/10.1175/1520-0442(2003)016<2653:tsfmit>2.0.co;2

Vimont, D., Wallace, J., & Battisti, D. (2003). The seasonal footprinting mechanism in the Pacific: Implications for ENSO. *Journal of Climate*, *16*, 2668–2675. https://doi.org/10.1175/1520-0442(2003)016<2668:tsfmit>2.0.co;2

Vimont, D. J., Battisti, D. S., & Hirst, A. C. (2001). Footprinting: A seasonal connection between the tropics and mid-latitudes. *Geophysical Research Letters*, *28*(20), 3923–3926. https://doi.org/10.1029/2001GL013435

You, Y. J., & Furtado, J. C. (2017). The role of South Pacific atmospheric variability in the development of different types of ENSO. *Geophysical Research Letters*, *44*(14), 7438–7446. https://doi.org/10.1002/2017GL073475

Zhang, H., Clement, A., & Di, N. P. (2014). The South Pacific meridional mode: A mechanism for ENSO-like variability. *Journal of Climate*, *27*(2), 769–783. https://doi.org/10.1175/jcli-d-13-00082.1

Zhang, L., Chang, P., & Ji, L. (2009a). Linking the Pacific meridional mode to ENSO: Coupled model analysis. *Journal of Climate*, *22*(12), 3488–3505. https://doi.org/10.1175/2008JCLI2473.1

Zhang, L., Chang, P., & Tippett, M. K. (2009b). Linking the Pacific meridional mode to ENSO: Utilization of a noise filter. *Journal of Climate*, *22*(4), 905–922. https://doi.org/10.1175/2008JCLI2474.1

Zhang, Y., Wallace, J. M., & Battisti, D. S. (1997). ENSO-Like interdecadal variability: 1900–93. *Journal of Climate*, *10*(5), 1004–1020. https://doi.org/10.1175/1520-0442(1997)010,1004:ELIV.2.0.CO;2

Zhao, Y., & Di Lorenzo, E. (2020). The impacts of extra-tropical ENSO precursors on tropical Pacific decadal-scale variability. *Scientific Reports*, *10*(1), 12. https://doi.org/10.1038/s41598-020-59253-3

Zhao, Y., Di Lorenzo, E., Newman, M., Capotondi, A., & Stevenson, S. (2023). A Pacific tropical decadal variability challenge for climate models. *Geophysical Research Letters*, *50*(15), e2023GL104037. https://doi.org/10.1029/2023gl104037

Zhao, Y., Di Lorenzo, E., Sun, D., & Stevenson, S. (2021). Tropical Pacific decadal variability and ENSO precursor in CMIP5 models. *Journal of Climate*, *34*(3), 1023–1045. https://doi.org/10.1175/JCLI-D-20-0158.1

Zhao, Y., Newman, M., Capotondi, A., Di Lorenzo, E., & Sun, D. (2021). Removing the effects of tropical dynamics from North Pacific climate variability. *Journal of Climate*, *34*(23), 9249–9265.